Chapter 10
Phytomediated Synthesis of Cerium Oxide Nanoparticles and Their Applications

Annu, Akbar Ali, Rahul Gadkari, Javed N. Sheikh, and Shakeel Ahmed

Abbreviations

AZO	Azodicarbonamide
CeO NPs	Cerium oxide nanoparticles
CeO_2	Cerium dioxide
DSC	Differential scanning calorimetry
FESEM	Field emission scanning electron microscopy
ROS	Reactive oxygen species
SAED	Selected area electron diffraction
SEM	Scanning electron microscopy
STM	Scanning tunnelling microscopy
TEM/HRTEM	Transmission electron microscopy/high-resolution transmission electron microscopy
TGA	Thermogravimetric analysis
WAXD	Wide-angle X-ray diffraction
XPS	X-ray photoelectron spectroscopy
XRD	X-ray diffraction

10.1 Introduction

Among the rare earth group elements, cerium is most abundant. Out of the 83 naturally occurring elements in the earth lithosphere, cerium ranks 28th position in its abundance. Jons Jakob Berzelius and Wilhelm Hisinger discovered cerium in

Annu · A. Ali
Department of Chemistry, Jamia Millia Islamia, New Delhi, India

R. Gadkari · J. N. Sheikh
Department of Textile Technology, Indian Institute of Technology, New Delhi, India

S. Ahmed (✉)
Department of Chemistry, Government Degree College Mendhar, Mendhar, Jammu, India

A. Husen, M. Iqbal (eds.), *Nanomaterials and Plant Potential*,
https://doi.org/10.1007/978-3-030-05569-1_10

Bastnas (Sweden) in 1803 and by Martin Heinrich Klaproth in Germany. Later, Berzelius and Hisinger proposed the name ceria to cerium in honour of the newly sighted asteroid Ceres (Weeks 1932; Dahle and Arai 2015). The main sources of cerium are allanite, bastnasite, monazite and cerite. Allanite, a silicate comprising of rare earth elements, aluminium, calcium and iron, is found extensively in Germany, Greenland, Madagascar, Scandinavia and the United States. Bastnasite, the most important commercial source of cerium and other light rare earth elements existing essentially as a rare earth fluorocarbonate, is found in Southern California. Cerite contains calcium and iron rare earth silicate and belongs mainly to Sweden. It has a high ratio of rare earth contents, but not enough to be the primary source of cerium. Monazite is a phosphate and another major source of cerium; it contains thorium and other light rare earth elements. Its main deposits are located in Australia, Brazil, the United States (Idaho and Florida), South Africa and India (Enghag 2004).

Physically, cerium is soft and ductile. In pure form, cerium has silver colour, but the commercial grade cerium is iron-grey. The pure cerium ignites, if scratched with a sharp object. Moreover, it tarnishes readily in the air, oxidizes rapidly in hot water, dissolves in acids and can burn when heated (Kilbourn 2000). Cerium dioxide (CeO_2) is a crystalline material and a major compound in the rare earth family. It has gained much attention owing to its numerous unique characteristics, such as high temperature stability, high hardness index, ultraviolet radiation-absorbing ability and its reactivity (Trovarelli et al. 1999). With the rapid progress in nanotechnology these days, nanoparticles (NPs) are now being used in various manufacturing, remedial and therapeutic processes. Cerium oxide nanoparticles (CeO NPs), also known as nanoceria, are very popular for their multifarious applications in several industries and are being synthesized in a variety of ways, which will be examined in this chapter.

10.2 Methods of Synthesis of Cerium Oxide Nanoparticle

The methods used in the synthesis of NPs play significant role in determining the morphological and structural properties of these particles. Some researchers preferred the solvothermal technique to synthesize the CeO_2 NPs so as to control conveniently their structural and morphological features. Cerium (IV) ammonium nitrate and sodium hydroxide in 1:4 molar ratio were dissolved in deionized water to form a solution of pH 12. The whole mixture was stirred for 1 h, using a magnetic stirrer with a stirring rate of 1000 rpm, and then kept in microwave oven for 30 min at 50 °C. The treatment of ammonium ceric nitrate with sodium hydroxide initiates hydrolysis, leading to the formation of products like ammonium hydroxide, cerium hydroxide and sodium nitrate. Due to the polar nature of water, a proton (H^+) gets removed from cerium hydroxide during the course of reaction, leading to the formation of hydrated CeO_2. Annealing of the hydrated CeO_2 at 800 °C for 6 h resulted in the formation of CeO_2 NPs. The particle size varies between 10 and 75 nm with an average size of 20 nm. The NPs showed good thermal stability and insulating

property with a slight increase in conductivity (AC) on increasing the temperature (Kumar et al. 2013).

In another study, CeO_2 NPs were prepared from cerium nitrate as the starting material and sodium hydroxide (NaOH) as the precipitating agent, without using any stabilizer in the conventional or the sonochemical precipitation method. In the conventional method, NaOH solution (0.3 gmol) was added dropwise to 30 mL cerium nitrate hexahydrate solution (0.1 gmol) under constant stirring at 35 ± 2 °C, giving a yellowish white solution. The reaction converted the yellowish white solution to a light yellow colloidal suspension. After the completion of reaction (4 h), the solution was centrifuged to separate the product and heated at 100 °C for 3 h to get CeO_2 (light yellowish powder) from $Ce(OH)_3$ (Pinjari and Pandit 2011). The same concentrations of cerium nitrate hexahydrate and NaOH were used for the synthesis of CeO_2 by the sonochemical method, where the solutions were mixed under sonication by an ultrasonic horn (CE 22 kHz, 40% amplitude) for 2 min with a 5 s pulse and 5 s relaxation cycle at 35 ± 2 °C temperature. The addition was done in concurrence with the sonic pulse generated by the transducer, followed by the exposition of the solution to acoustic cavitation again for 18 min at constant sonication parameters. The remaining procedure was the same as in the conventional method.

The sonochemical method provides a simple, convenient, fast, economical and environmentally benign technique with more than 92% (15.15×10^{-2} kJ/g for sonochemical and 200.43×10^{-2} kJ/g for conventional method) energy saving for the synthesis of CeO_2. The crystallite size obtained in both cases was below 30 nm.

The ultrafine ceria particles of less than 5 nm size were synthesized using the conventional hydrothermal methods, employing the tetravalent cerium salts [$Ce(SO_4)_2$), $(NH_4)_2Ce(NO_3)_6$ and $Ce(NH_4)_4(SO_4)_2$] as starting materials. However, high surface energy of the nanoparticle caused agglomeration followed by precipitation, which makes it difficult to synthesize well-dispersed particles. The presence of SO_4^{2-} ions in the solution further accelerates the agglomeration processes. Protection of the NP surface will make it possible to control the size and agglomeration. The addition of citric acid molecules controls the size of cerium oxide NPs and the agglomeration process via adsorption on the surface of the particle (Hirano et al. 2000; Masui et al. 2002).

Another study suggested a new method to obtain ultrafine as well as well-dispersed CeO_2 NPs through the application of citric acid as a shielding agent against particle growth using a 1:1 molar ratio of cerium chloride (1 M aqueous solution) and citric acid adding to an excess amount of 3 M ammonium water. A dark brown transparent liquid was attained after stirring for 24 h at 323 K. The product particles were crystallized via transferring the transparent liquid and heated at 353 K for 24 h in a Teflon bottle kept in a vessel. Although the apparent status of the liquid did not change by heat treatment, the crystallinity after the treatment became higher than before. The brown liquid started showing Tyndall effect, indicating the presence of well-dispersed colloidal particles. The resulting NPs were separated by centrifugation (centrifugal force 4.1×10^4 g and 2.1×10^4 pm) for 24 h, washed with water and dried by a freeze-drying method (Masui et al. 2002).

A relatively fast "microwave hydrothermal" method has also been devised for the fast synthesis of nanoceria and nanorods. This reportedly energy-saving, high-yielding, rapid and environment-friendly method had the collective advantages of hydrothermal as well as microwave-heating techniques and produced the CeO_2 NPs of the average size of 1.6–20 nm. Besides, CeO_2 nanorods could be synthesized by altering the cerium source and regulating the quantity of the added ammonia water (Gao et al. 2006). Some researchers prepared CeO NPs by mixing the $Ce(NO_3)_3$ (0.0375 M) and hexamethylenetetramine (0.5 M) solutions in equal volumes at room temperature. Bunches of particles ranging in size between 3 and 12 nm were obtained by controlling the reaction time (Zhang et al. 2002). Nanoceria of an average particle size of 3.3 nm were also obtained sonochemically, using tetramethyl ammonium hydroxide as additive, having a molar ratio of starting materials and additives in 1:1:1. Cerium nitrate and azodicarbonamide (AZO) were used as the starting materials along with ethylenediamine or tetraalkyl ammonium hydroxide as the additive. Typically, 0.1 g AZO was added to a solution of $Ce(NO_3)_3$ (0.434 g in 50 mL distilled water) followed by the addition of varied extents of additives that showed strong influence on the size and distribution of particles. Addition of additives resulted in the production of small-sized particles of CeO_2 with a narrow range of distribution, whereas agglomerated nanoparticles were obtained without using additives (Yin et al. 2002).

10.3 Techniques Used for Characterization of Nanoparticles

10.3.1 NP Characterization by Spectroscopy

10.3.1.1 UV-Visible Spectroscopy

Ultraviolet-visible (UV-Vis) spectrophotometer consists of a source of light (xenon lamp), sample beam, reference beam, a monochromator and a detector. The UV-Vis spectra for a compound are achieved by exposing a dilute solution of the sample to UV light. Metallic nanoparticles, normally of 40–100 nm, scatter optical light elastically with significant efficiency due to a phenomenon known as surface plasmon resonance, which is a collective resonance of the conduction electrons in the metal. The intensity, peak position and spectral bandwidth of the plasmon resonance related with a nanoparticle depend on the NP composition and dimensions like shape and size. For example, Fig. 10.1a shows a typical UV-vis spectrum of CeO NPs displaying their characteristic absorption peak at a wavelength (λ max) of 345 nm. The NPs synthesized via solvothermal route were found to have the maximum absorbance at wavelength 317 nm. Phytomediated synthesized nanoceria display λmax at 345 nm generally due to the intrinsic band gap absorption, which owes to the electronic transitions from valence band [O(2p)] to the conduction band [Ce(4f)] in the nanoceria. Band gap of CeO_2 was reported to be 3.19 eV (Fig. 10.1b), whereas band gap of nanoceria was estimated around 3.59 eV. The increase (0.40 eV) in band gap might be owing to the reduction in particle size or change in oxidation state (Ce^{3+} to Ce^{4+}) (Patil and Paradeshi 2016).

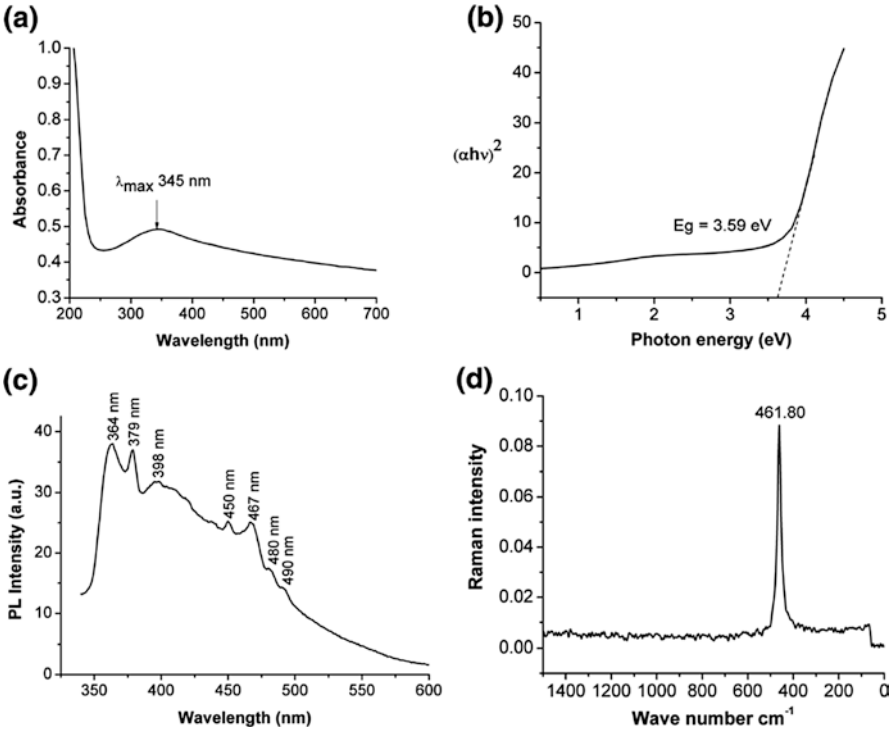

Fig. 10.1 (**a**) UV-visible spectra of CeO NPs, (**b**) photon energy level, (**c**) photoluminescence spectra recorded under light excitation wavelength 320 nm, (**d**) Raman spectra of CeO NPs synthesized using pectin (Patil and Paradeshi 2016)

10.3.1.2 Photoluminescence

Photoluminescence is the light emission from any form of matter after absorption of photons. The time periods between absorption and emission may vary ranging from femtoseconds to milliseconds. This process can be categorized on the basis of energy of exciting photon w.r.t. the emission. Green synthesized CeO NPs exhibited strong emission peaks starting from a shorter wavelength (360 nm) to a longer one (500 nm). The typical photoluminescence spectrum of CeO NPs recorded at an excitation wavelength of 320 nm is shown in Fig. 10.1c. The emission spectra displayed four bands in blue-green region (450, 467, 480 and 490 nm) and three bands in the near band edge of wavelength (364, 379 and 398 nm), respectively. The near band edge was attributed to the localized or free excitons, and blue region peaks were attributed to the bouncing of electrons from localized [Ce(4f)] state to the [O(2p)] valence band. Besides, the green peaks were ascribed to the surface defects in CeO NPs, whereas low density of oxygen vacancies caused weak intensities (Patil and Paradeshi 2016). The same was exhibited by the *Gloriosa superba* leaf extract-mediated nanoceria (Arumugam et al. 2015a). Another study reported the

excitation spectra of nanoceria by monitoring the emission at 425 nm. It comprised of a sharp peak at 388 nm, attributed to Ce^{4+} intra-configuration (f–f) transitions (Malleshappa et al. 2015).

10.3.1.3 Raman Spectroscopy

It is a low-frequency spectroscopy technique, mainly used in the condensed matter physics and chemistry to study the rotational, vibrational and other low-frequency modes in a system. In chemistry, it is used normally as an indicator of vibrational frequency change, which is highly specific for the chemical bonds in molecules. It gives information in the fingerprint region (500–2000 cm^{-1}) of a molecule, which can be helpful in the identification of unknown molecules. For CeO NPs, a strong and broad Raman active mode band appears at 461.1 cm^{-1} in Fig. 10.1d, which might be ascribed to the symmetrical stretching mode of Ce-O8 vibration unit (Patil and Paradeshi 2016).

10.3.1.4 Fourier Transform Infrared (FT-IR) Spectroscopy

FT-IR technique utilizes high spectral resolution data over a wide spectral range. This can be applied to get an infrared spectrum of absorption or emission of a solid, liquid or gas. FT-IR has remarkable advantage over dispersive spectrometer. Besides, it is an analytical technique used to detect the base polymer composition, functional group and organic contaminants. It uses infrared light to probe the test samples and observe their chemical properties. The FT-IR spectra of Indian red pomelo extracted pectin-mediated CeO NPs showed the characteristic peaks as shown in Fig. 10.2 and Table 10.1. An additional peak has also been observed at 545 cm^{-1} for Ce-O stretching vibration for cubic cerium oxide (Kumar et al. 2013). On the other hand, annealed nanoceria depicted a sharp peak at 558 cm^{-1} for Ce-O stretching vibrations along with 3397, 1624 and 1471 cm^{-1}, which were due to water and CO_2 taken up from the atmosphere (Patil and Paradeshi 2016).

10.3.2 NP Characterization by Microscopy

Optical microscopy techniques are used commonly for observing particles at micron level with reasonable magnification. However, higher magnification processing is not possible through ordinary optical microscopes due to aberration and limitations in wavelength of light. Therefore, advanced imaging techniques such as scanning electron microscopy (SEM), transmission electron microscopy/high-resolution transmission electron microscopy (TEM/HRTEM) and scanning tunnelling microscopy (STM) are used to analyse the surface structure and internal morphology (size, shape and dimensions) of nanoparticles with due clarity.

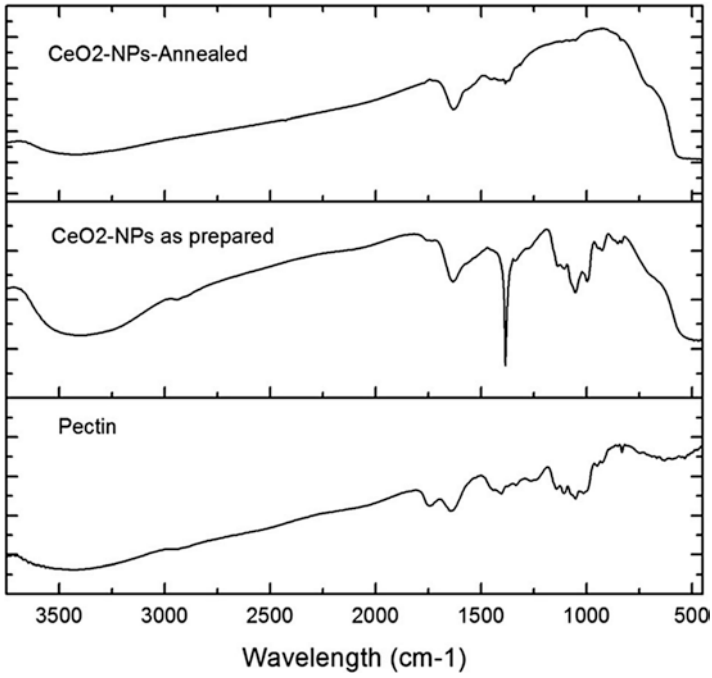

Fig. 10.2 FT-IR spectra of pectin, CeO NPs prepared using pectin and CeO NPs annealed (Patil and Paradeshi 2016)

Table 10.1 Characteristic FT-IR peak of CeO NPs (Patil and Paradeshi 2016)

S. No	IR frequency (cm^{-1})	Functional group present
1	3390	-OH, stretching
2	2939	C-H, stretching of methyl ester of galacturonic acid
3	1738	C=O, stretching vibration of methyl-esterified carboxyl group
4	1634	C=O, stretching vibration of carboxylate group
5	1402	C-O-H, in plane bending vibration
6	1295	C-O-C, asymmetric stretching vibration of $–O-CH_3$ group
7	1105	C-O-C, bending mode of acetal group
8	1051	C-O-C, bending mode of ethereal group
9	955	Glycosidic group

10.3.2.1 Scanning Electron Microscopy (SEM)

Scanning electron microscopy involves scanning of the surface of a sample with a focused beam of electrons which interacts with the atoms of the sample, producing various signals. These signals possess the sample's information about surface topography and composition. In the case of CeO NPs obtained from Indian red

pomelo pectin, field emission scanning electron microscopy (FESEM) micrographs illustrated the shape of these NPs as spherical and agglomerated with their size ranging from 5 to 40 nm (Fig. 10.3), whereas the solvothermal gave the result as shown in Fig. 10.4. Additionally, the EDX pattern of CeO NPs revealed the presence of Ce, Au, O and C as the main components of the CeO NPs produced. The presence of Au and C in the EDX spectra appears due to the conductive carbon tape used to hold the sample and to the gold used for coating the sample (Patil and Paradeshi 2016).

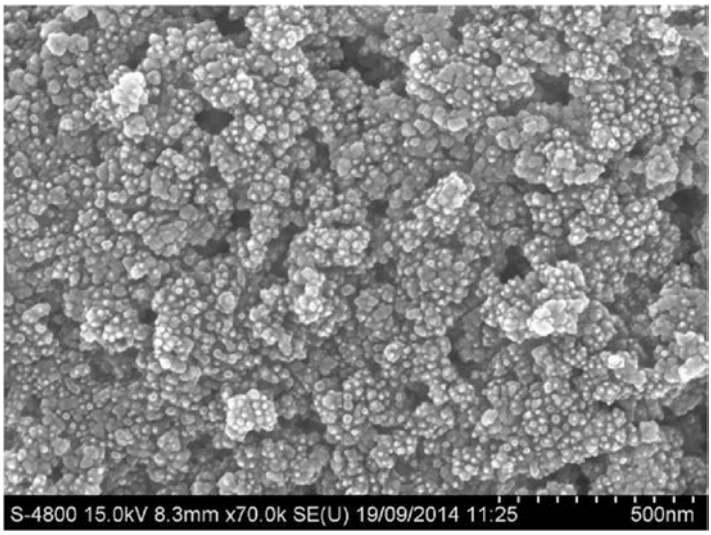

Fig. 10.3 FESEM micrograph of CeO NPs synthesized using pectin (Patil and Paradeshi 2016)

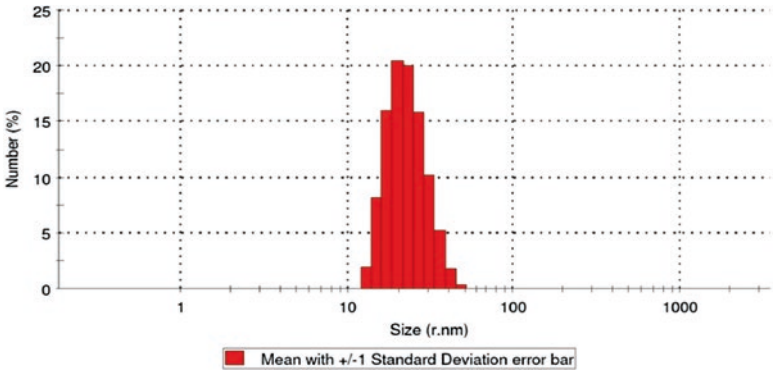

Fig. 10.4 Particle size distribution histogram of biopolymer-mediated CeO NPs (Patil and Paradeshi 2016)

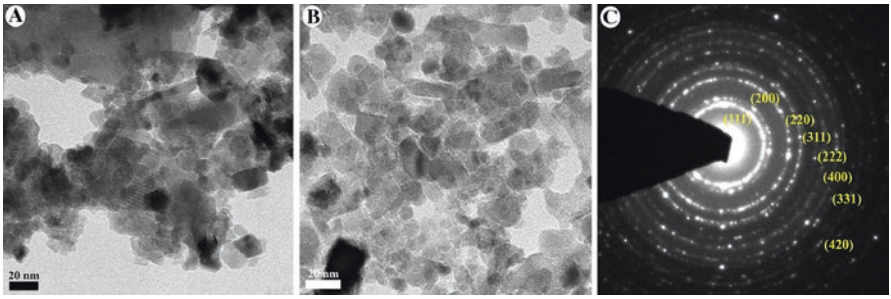

Fig. 10.5 (**a**) TEM images of mycosynthesized CeO NPs (**b**) calcined at 40 °C and (**c**) SAED of CeO NPs (Gopinath et al. 2015a, b)

10.3.2.2 Transmission Electron Microscopy (TEM)

TEM is a technique in which a beam of electrons is transmitted through a sample to form an image and the image is further magnified on a fluorescent screen. Briefly, TEM is generally used for imaging the structural details at a significantly higher resolution. The structure of CeO NPs can be observed with TEM (K. Gopinath, V. Karthika, C. Sundaravadivelan, S. Gowri 2015a). The HRTEM images showed that CeO NPs possessed spherical and cubic morphology and their size ranged between 5 and 20 nm with an average particle size of nearly 10 nm. The nanoparticles also showed fluorite cubic structure having a characteristic ring pattern in the selected area electron diffraction (SAED) and possessed a high degree of crystallinity (Fig. 10.5).

10.3.3 TGA/DTA Analysis

Thermal stability of the crystalline samples can be examined using the differential thermal analysis techniques (thermogravimetric and differential scanning calorimetry) under high temperature. The thermal stability of green synthesized nanoparticles of CeO_2 has been analysed in the temperature range of 35–1000 °C at a heating rate of 20 °C per min. A TGA/DTA curve of CeO NPs is shown in Fig. 10.6. The NPs exhibit a three-stage decomposition pattern, with the first stage accompanied by a 9.84% weight loss at 35–100 °C due to dehydration of water, moisture and extracellular fungal components, the second stage contributes a weight loss of 13.49% from 100 to 150 °C, and the third stage shows the maximum weight loss of 15.25% at the temperature range of 540–1000 °C. On DTA curve, the exothermic peaks observed at 115 °C were attributed to the combustion of organic residues, and those at 615 °C were ascribed to oxygen loss at higher temperatures and decomposition of some residual, absorbed species. Moreover, the phase change or variation in the oxidation state of cerium was shown by a slight increase in the DTA curve above 740 °C (Gopinath et al. 2015b).

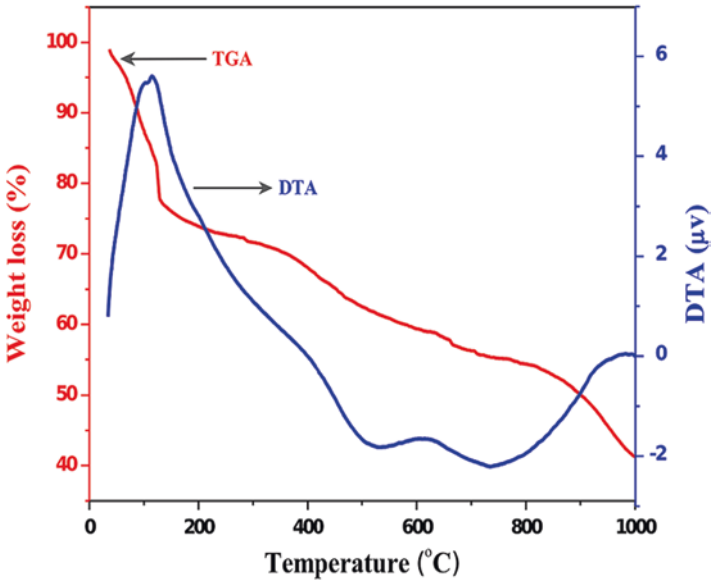

Fig. 10.6 TGA/DTA curves of green synthesized CeO_2 nanopowders (Gopinath et al. 2015a, b)

10.3.4 NP Characterization by X-Ray Technique

X-ray diffraction (XRD) technique gives information about the crystallinity, crystal size, phase composition, and crystal alignment. Two types of X-ray technique are generally used in the characterization of nanoparticles:

1. Wide-angle X-ray diffraction (WAXD): It provides information about the crystallinity, alignment of the crystal, crystallite size and the phase composition in semi-crystalline polymer.
2. X-ray photoelectron spectroscopy (XPS): This quantitative surface chemical analysis spectroscopic technique is used to evaluate the elemental composition or empirical formula, electronic state and chemical state of the elements on the surface up to 10 nm of a material. It also detects the presence of contaminants on the surface of the sample and oxidation state of each element present in the sample with the composition of the surface functionalization of the CeO NPs.

Hewer et al. (2013) prepared CeO NPs surrounded by carbon microspheres by utilizing D(+)-glucose in the one-pot green hydrothermal process. In XRD analysis, five diffraction peaks at 2θ = 28.5, 33.0, 47.4, 56.3 and 76.6° were observed and attributed to the (111), (200), (220), (311) and (331) cubic plane of CeO_2 (JCPDS 34-0394), respectively. The diffraction peak showed the face-centred cubic phase of nanoceria (Hewer et al. 2013). Another study revealed some other peaks at 2θ = 59.09, 69.0 and 78.99°, attributed to (222), (400) and (420) planes of

face-centred cubic nanoceria, respectively. Debye-Scherrer's formula was applied to calculate the average crystallite size of CeO NPs which came out to be 24 nm (Arumugam et al. 2015b).

10.3.5 Particle Size Analyser

Dynamic light-scattering techniques are generally coupled with various other techniques such as sieve analysis, electro-resistance counting method, laser diffraction method and optical counting method for the determination of particle size and distribution. A general particle size distribution histogram showing the CeO NPs having a hydrodynamic size (*Z*-average) distribution (around 29.47 nm) is presented in Fig. 10.4 (Patil and Paradeshi 2016).

10.4 Green Synthesis of Cerium Oxide Nanoparticles or Nanoceria

The term "green" is used to indicate an eco-friendly and environmentally benign use of the less energy-consuming, non-toxic chemicals and the bio-derived products for the synthesis of NPs (Husen 2017; Siddiqi and Husen 2017; Siddiqi et al. 2018). The nanoceria have been prepared using several ways and means such as solution precipitation; hydrothermal, solvothermal or thermal decomposition; thermal hydrolysis; and spray pyrolysis methods. But these methods have several disadvantages, like the use of toxic solvents and reagents, high pressure and temperature and the external additives (stabilizing or capping agents) during the reaction. Figure 10.7 displays various physical, chemical and physicochemical methods of the synthesis of nanoparticles, highlighting the green or biological approaches. Numerous bio-directed approaches involving application of natural products and other organic matrices as a stabilizer are now being used to obtain the biocompatible nanoceria. Phytosynthesis of metals and metal oxide nanoparticles is a novel subject in nanoscience engineering. Of late, phytosynthesis of nanoceria, using the extracts of plant species (such as *Aloe vera*, *Acalypha indica* and *Gloriosa superba*) as stabilizing and capping agents, has been reported (Kannan and Sundrarajan 2014; Priya et al. 2014; Arumugam et al. 2015a). Tables 10.2 and 10.3 indicate the source materials, methods for green synthesized nanoceria and also the reported advantage/disadvantage associated with these methods, respectively.

Leucas aspera leaf extract-mediated nanoceria have been characterized under diffraction technique, and the patterns (111), (200), (220) and (222) were well indexed to a pure cubic fluorite structure of CeO NPs (JCPDS Card No. 81-0792) without any impurity peak, thus indicating the single phase of CeO NPs. The study further concluded that the concentration of leaf extract strongly influences the structural parameters such as crystallite size and lattice constant (Malleshappa et al. 2015).

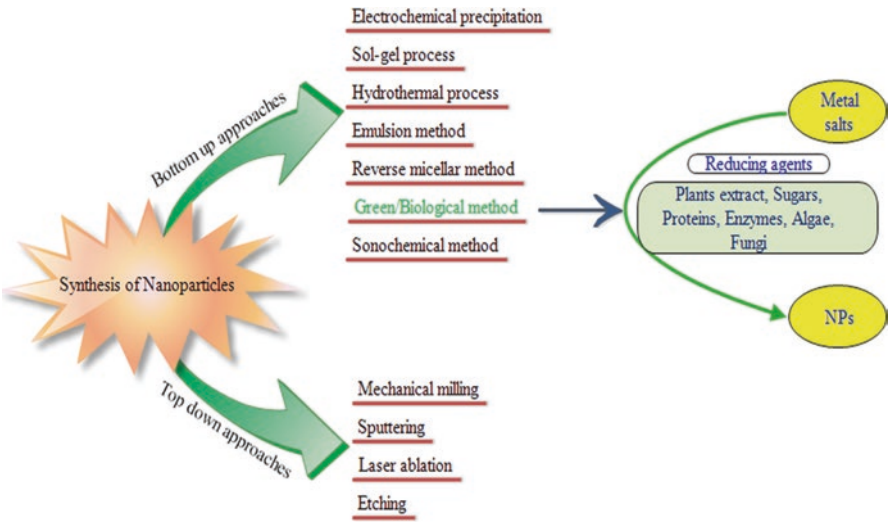

Fig. 10.7 Generalized representations of various physicochemical methods of nanoparticle synthesis, emphasizing the biological synthesis

Besides, Patil and co-workers have synthesized CeO NPs using a non-toxic biopoly-

Table 10.2 Green synthesis methods for CeO NPs

Green synthesis methods used	Materials used	Particle size (nm)	Morphology	References
Plant-mediated	*Gloriosa superba*	5	Spherical	Arumugam et al. (2015a)
Plant-mediated	*Centella asiatica*	8	Spherical and monodisperse	Sankar et al. (2015)
Plant-mediated	*Acalypha indica*	36	Spherical	Kannan and Sundrarajan (2014)
Plant-mediated	*Piper longum*	46	Spherical	Reddy Yadav et al. (2016)
Plant-mediated	China rose petal	7	Nanosheet	Qian et al. (2011)
Plant-mediated	*Aloe vera*	18.23	Spherical	Tamizhdurai et al. (2017)
Fungus-mediated	*Curvularia lunata*	5–20	Spherical	Munusamy et al. (2014)
Nutrient-mediated	Egg white	6–30	Plate like	Maensiri et al. (2007)
Nutrient-mediated	Honey	23	Spherical	Darroudi et al. (2014a)
Biopolymer-mediated	Agarose	10.5	Spherical	Mittal and Pandey (2014)
Biopolymer-mediated	Starch	6	Spherical	Darroudi et al. (2014b)
Biopolymer-mediated	Gum	10	Spherical	Charbgoo et al. (2017a)
Biopolymer-mediated	Dextran	10	Spherical	Perez et al. (2008)
Biopolymer-mediated	Pectin	≤40	Spherical	Patil and Paradeshi (2016)
Biopolymer-mediated	Chitosan	~4	Spherical	Sifontes et al. (2011)

Table 10.3 Advantages and challenges encountered by the green methods for the synthesis of CeO NPs

Green methods	Advantage	Disadvantage/challenge	Reference
Plant-mediated synthesis of CeO NPs	Spherical-shaped NPs were obtained with reduced cytotoxicity Easy process, cost-effective, energy- and time-efficient technique Capable of producing stable, water-dispersible, and highly fluorescent NPs	Non-uniformity in morphology in some cases due to which agglomeration of the individual NPs occurs Size of NPs exhibited wide distribution range from 5 to 63.6 nm, using different bio-organisms for synthesis	Gopinath et al. (2015a, b), Charbgoo et al. (2017b)
Nutrient-mediated synthesis of CeO NPs	Controllable growth and subsequent isotropic formation of small and stable CeO NPs	Lack of information about the constituents accountable for metal ions reduction	Reddy Yadav et al. (2016), Charbgoo et al. (2017b)
	Capable of providing spherical CeO NPs with narrow distribution range of particle size		
	Synthesized CeO NPs non-toxic toward human cell lines at physiological concentrations of NPs		
Biopolymer-mediated synthesis of CeO NPs	Generating NP with spherical morphology	Reproducibility of the methods need to be enhanced Abundance of structural components might affect the synthesis procedure Complete elucidation of mechanism is still a major challenge	Primo et al. (2011), Sun et al. (2012), Darroudi et al. (2014c), Kargar et al. (2015), Sathiyanarayanan et al. (2017)
	Providing NPs with no significant cytotoxic effect in human cell line at physiological concentrations		
	Capable of controlling diameter of CeO NPs		
	Providing NPs with high final purity		

mer pectin. The Braggs peaks are found at an angle (2θ) of 28.51, 33.06, 47.42, 56.30, 59.09, 69.00, 76.57 and 78.99° with Miller indices (111), (200), (220), (311), (222), (400), (331) and (420), respectively (Fig. 10.8). The synthesized CeO NPs exhibited a pure cubic fluorite structure (space group, Fm-3 m, 225), which is in agreement with the JCPDS PDF 00-033-0334. The lattice value and the unit cell volume were 5.089 Å and 131.795 Å, respectively. Furthermore, the average crystallite size of the phyto-mediated CeONPs was estimated to be 23.71 nm using the Debye-Scherrer equation (Patil and Paradeshi 2016).

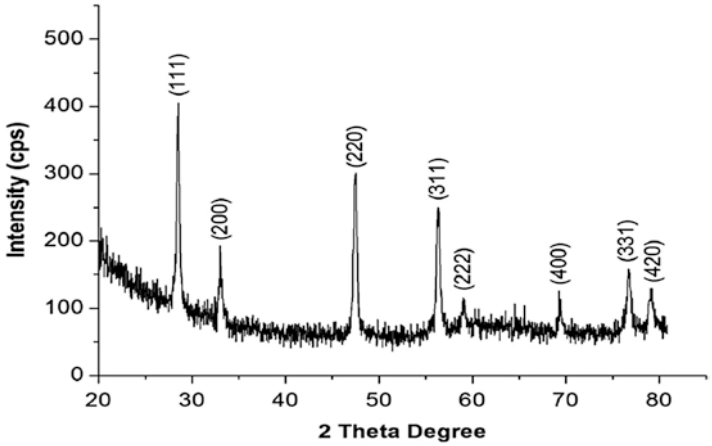

Fig. 10.8 X-ray powdered diffraction pattern of pectin-mediated synthesized CeO NPs (Patil and Paradeshi 2016)

10.5 Applications of CeO NPs

Nanoceria have the potential to be utilized in various areas of science and technology and are being used in paint industry, glass polishing, fuel additives, supercapacitors, emission control or biodiesel, biogas production, biosensing, microcosm system for soil, cosmetics, coating and most commonly biomedical sciences. However, the biomedical applications of nanoceria require a lot of care and precaution (Castano et al. 2015; Nguyen et al. 2015; Walkey et al. 2015; Oró et al. 2016; Charbgoo et al. 2017b; Li et al. 2017; Vinothkumar et al. 2017).

10.5.1 Biomedical Applications

10.5.1.1 Anti-inflammatory

Chronic inflammation, a complex immunological ailment caused by the increased levels of nitric oxide, results in irreversible organ dysfunctioning or damage. It often leads to major diseases such as cardiac disorder, rheumatoid arthritis, atherosclerosis and multiple sclerosis. Cerium oxide NPs have been used for the treatment of such chronic inflammation (Hirst et al. 2009). Khan and Ahmad have successfully synthesized CeO NPs by using the thermophilic fungus *Humicola sp.* for utilization in biomedical sciences. The fungus-secreted capping protein, involved in the capping of nanoparticles, made the particles highly stable, non-agglomerate, highly fluorescent and, most importantly, water dispersible (Khan and Ahmad 2013).

10.5.1.2 Antibacterial Activity

The nanoceria fabricated via green route exhibit good antibacterial and antifungal activity against pathogens in the oxidation states +III and +IV (Annu and Ahmed 2018). Some researchers synthesized them using the leaf extract of *Gloriosa superba* and studied the formed nanoparticles against Gram-positive and Gram-negative bacteria at varying concentrations. At high concentration of 100 mg, the zone of inhibition effect was the largest (5.33 mm) against *Staphylococcus aureus*. The *Escherichia coli* and *Shigella dysenteriae* exhibited a modulated effect on the inhibition zone of 4.00 mm and 4.33 mm, respectively. Then, *Pseudomonas aeruginosa*, *Proteus vulgaris*, *Klebsiella pneumonia* and *Streptococcus pneumoniae* showed similar inhibition zone of 4.67 mm for enhanced activity (Arumugam et al. 2015a). Similarly, the use of the leaf extract of *Acalypha indica* resulted in increased rate of antibacterial activity against Gram-positive and Gram-negative bacteria (Kannan and Sundrarajan 2014). Likewise, the nanoceria synthesized from the fungus *Aspergillus niger* showed antibacterial, larvicidal and pupicidal activities against human pathogens, viz. Gram-positive *Streptococcus pneumoniae* and *Bacillus subtilis* and Gram-negative *Proteus vulgaris* and *Escherichia coli* (Gopinath et al. 2015a, b). The authors obtained different results from different concentrations of nanoceria. For instance, 1 mg nanoceria per mL did not show any inhibition zone with any of the stains, while moderate zones of inhibition (4.67 ± 0.33 mm, 3.33 ± 0.33 mm, 3.67 ± 0.33 mm and 3.33 ± 0.33 mm) were observed in *B. subtilis*, *E. coli*, *P. vulgaris* and *S. pneumoniae* at 5 mg/mL concentration, respectively. However, at 10 mg mL^{-1} concentration of nanoceria, remarkable inhibition zones (10.33 ± 0.33 mm, 6.33 ± 0.33 mm, 8.33 ± 0.33 mm and 10.67 ± 0.33 mm) with *B. subtilis*, *E. coli*, *P. vulgaris* and *S. pneumoniae*, respectively (Figs. 10.9 and 10.10) (Gopinath et al. 2015a). Gusseme et al. (2010) reduced biogenic cerium by using the freshwater manganese-oxidizing bacteria (MOB) *Leptothrix discophora* or *Pseudomonas putida* MnB29 and demonstrated the antiviral activity of nanoceria by removing virus bacteriophage UZ1 from water due to the bacterial carrier matrix (Gusseme et al. 2010).

Patil and Paradeshi (2016) utilized pectin, extracted from Indian red pomelo fruit peels, as a renewable, non-toxic biopolymer in order to fabricate CeO NPs. They found that the biogenically synthesized nanoceria exhibited significant antibacterial property against *E. coli* and *Bacillus subtilis* at both 1 and 2 mM concentrations used (Fig. 10.11a) which was far better than one shown by the bulk and CeO_2 powder. In case of *B. subtilis*, cerium nitrate was not effective at both (1 and 2 mM) concentrations, whereas the bulk CeO_2 caused a slight reduction in survival at 2 mM concentration only (Fig. 10.11b) (Patil and Paradeshi 2016).

Causes and Mechanism

The nanoceria exhibited a higher antibacterial activity against the Gram-positive than against the Gram-negative bacteria. This is because the cell wall of Gram-positive bacteria is composed of peptidoglycan which is attached to teichoic acids.

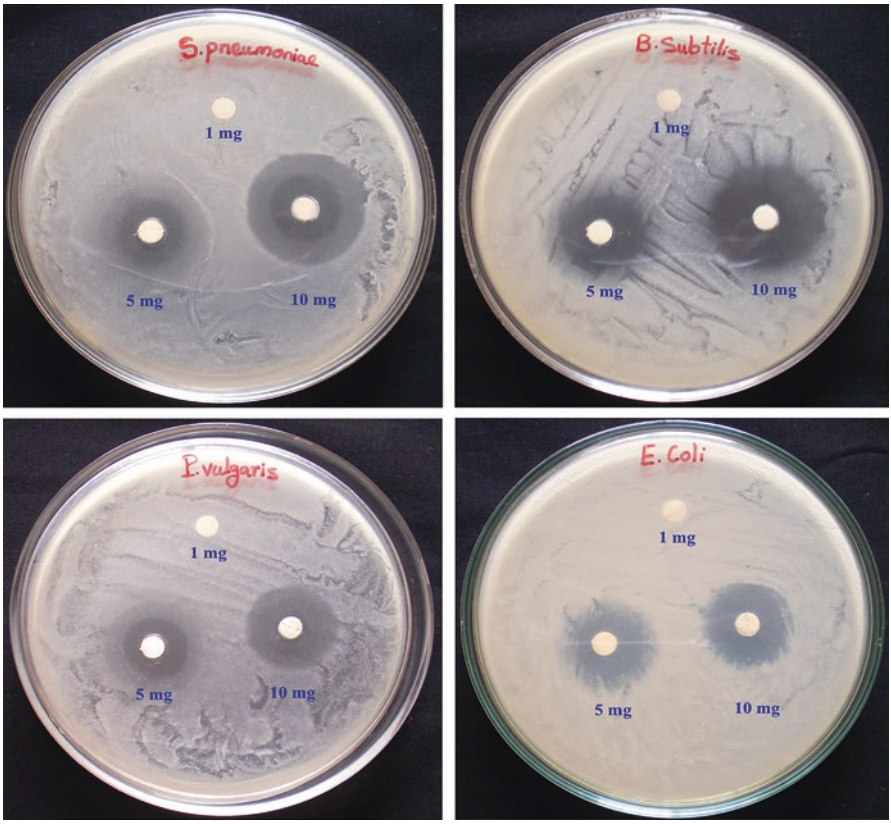

Fig. 10.9 Zones of inhibition by CeO_2 NPs at different concentrations against Gram-positive and Gram-negative bacteria (Gopinath et al. 2015a, b)

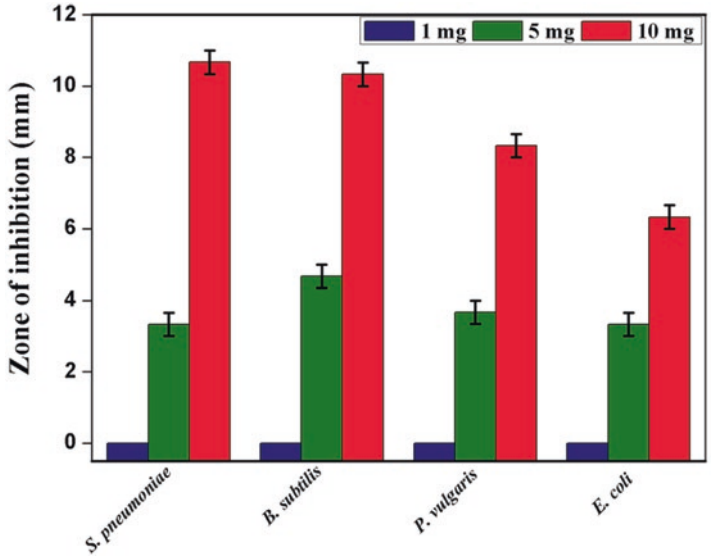

Fig. 10.10 Antibacterial activities of CeO_2 NPs against Gram-positive and Gram-negative bacteria (Gopinath et al. 2015a, b)

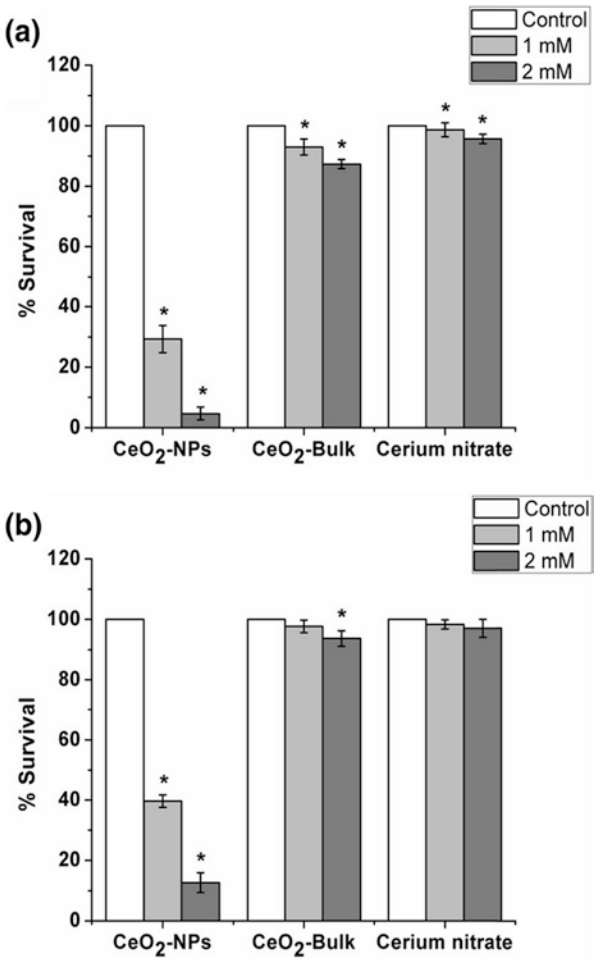

Fig. 10.11 Antibacterial activity of CeO NPs, bulk CeO_2 and cerium nitrate against (**a**) *E.coli* and (**b**) *B. subtilis*, expressed in terms of %age of the survival relative to the control group. In a group, the bars not labelled with asterisk demonstrate values (means) that are significantly different from the control ($p \leq 0.05$) by Dunnett's comparison test (Patil and Paradeshi 2016)

The electrostatic interaction between the positively charged metal or metal oxide nanoparticles and the negatively charged bacterial cell wall causes disruption of the cell wall, simultaneously generates reactive oxygen species (ROS) and ultimately leads to the death of the bacterial cell (Gopinath et al. 2015a, b). Figure 10.12 shows the schematic view of the cellular uptake of nanoparticles in general and the mechanism of inducing toxicity against bacteria (Hussain et al. 2016).

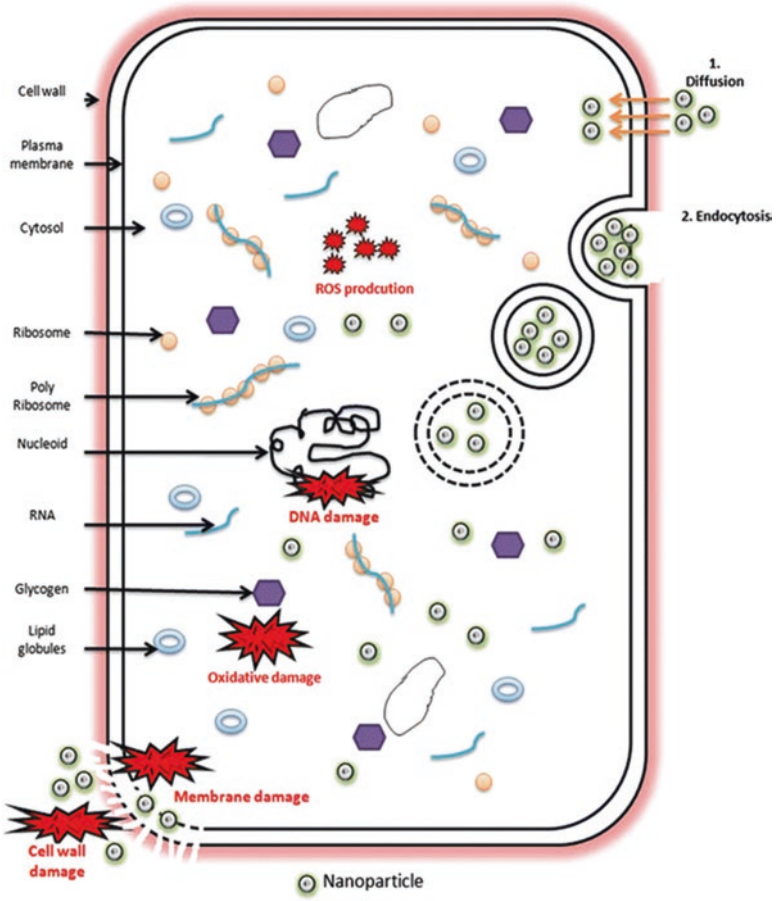

Fig. 10.12 Graphical representation of nanoparticle uptake by cells and the mechanism of toxicity induced by nanoparticles against bacteria (Hussain et al. 2016)

10.5.1.3 Cell Viability and Neurotoxicity

Agarose is a naturally occurring oxygen-rich straight-chain polysaccharide mined from red purple seaweeds. Some researchers have fabricated the CeO NPs by improved solgel route using the bioorganic agarose polymeric matrix, which acted as a stabilizing or capping agent. These biologically synthesized nanoparticles were then studied for cell viability on L929 cells at different concentrations varying from 0 to 800 μg mL^{-1}, and no significant cytotoxic effect could be observed at any concentration, suggesting that the biogenically synthesized nanoceria have the potential to be used in biomedical applications (Kargar et al. 2014). In another study, honey was used as a source to prepare CeO NPs with the help of solgel process at different

Table 10.4 Cytotoxicity of CeO NPs measured by the erythrocyte haemolysis assay (Patil and Paradeshi 2016)

S. No.	Sample	Optical density at 540 nm	% haemolysis
1	Distilled water	1.658 ± 0.028	100 ("+ve" control)
2	Physiological saline	0.034 ± 0.003	0 ("−ve" control)
3	CeO_2 NPs (0.50 mg/mL)	0.043 ± 0.003	0.55
4	CeO_2 NPs (1.00 mg/mL)	0.051 ± 0.006	1.05
5	CeO_2 NPs (2.00 mg/mL)	0.069 ± 0.005	2.16
6	CeO_2 NPs (4.00 mg/mL)	0.108 ± 0.008	4.55
7	CeO_2 NPs (4.00 mg/mL)	0.169 ± 0.008	8.31

calcinated temperatures, and their neurotoxic effect on the neuro2A cells was examined at concentrations ranging from 0 to 100 μg mL^{-1} (Darroudi et al. 2014a). It was found that the metabolic activity decreased in a concentration-dependent manner for more than 25 μg mL^{-1} after 24 h of incubation, thus proving to be more efficient in comparison to the conventionally produced nanoparticles (Darroudi et al. 2014a). In a study, based on the nanoceria synthesized with the help of pectin extracted from Indian red pomelo fruit peels, it was concluded after demonstrating the cell viability by erythrocyte haemolysis assay that the haemolysis (i.e. release of haemoglobin to plasma because of the rupture of erythrocyte membrane) increased when the concentration of nanoceria increased, as depicted in Table 10.4. This occurred at ≤4 mg mL^{-1}, which was within the permissible limit and hence biocompatible, but not much safe for human beings (Patil and Paradeshi 2016).

10.5.1.4 Antiobesity

Obesity leads to several pathologies such as type 2 diabetes, insulin resistance, cancer, hypertension and atherosclerosis. Commercially available drugs cause many side effects such as headache and insomnia. Nanoceria can strongly scavenge the ROS production for long duration and hence reduce the side effects. Rocca et al. (2015) studied the in vitro and in vivo cytotoxic effect of nanoceria on 3 T3-L1 pre-adipocytes and Wistar rats, respectively, in order to observe their interference in the lipid accumulation process and adipogenesis inhibition by reducing the mRNA transcription of genes involved in adipogenesis and by obstructing the triglyceride accumulation in 3 T3-L1 pre-adipocytes. Additionally, Wistar rats showed reduction in weight gain when injected with nanoceria; plasma level of insulin, glucose, leptin and triglycerides also declined, and no significant toxic effects appeared (Rocca et al. 2015). Another study revealed that the large surface area-to-volume ratio creates the oxygen defects as reactive sites on the nanoceria surface that can scavenge the free radicals generated in the biological system by inhibiting the ROS production and hence plays a vital role as antiobesity agent (Hirst et al. 2009).

10.5.2 Photocatalytic and Antioxidant Activity

Gogoi and Sarma (2017) biologically synthesized CeO NPs by solgel process using β-cyclodextrin in order to degrade efficiently the organic methylene blue dye from aqueous solutions at room temperature in the presence of H_2O_2 and absence of light irradiation. They found a complex pathway having different intermediates like leucomethylene blue, which is the reduced form of methylene blue and has $m/z = 286$; it is reduced further to leucomethylene blue sulfone having $m/z = 317$ amu. Thus, the colour of dye changes from blue to colourless, confirming the excellent photocatalytic activity of these nanoceria (Gogoi and Sarma 2017).

Leaf extract of *Aloe vera* was also used as stabilizing or capping agent to synthesize CeO NPs at ambient temperature (Dutta et al. 2016). The antioxidant property of nanoceria was found to be quite good which remained unaffected on being treated with H_2O_2 as the cerium was mainly present in (+III) oxidation state rather than (+IV) and the cyclic conversion took place from Ce(III)O → Ce(IV)O → Ce(III)O when reacted with H_2O_2. A gradual decrease in cell viability was noticed on increasing the H_2O_2 concentration (10–60 μM) for 24 h, and application of 4.34–78.16 μg mL^{-1} of CeO NPs remarkably enhanced cell viability, maximal at 120 μM, beyond which there was a decrease in the cell survival. Furthermore, a higher antioxidant activity and decrease of the lethal effects of H_2O_2 were observed with the higher oxygen defect in the crystal lattice. Thus, the biogenically synthesized nanoceria have the potential of being used as an antioxidant drug or a therapeutic agent for neural diseases triggered by oxidative stress and in other fields of biomedicine (Dutta et al. 2016). The catalytic properties of nanoceria, scavenging activity of nitric oxide radical, decay of peroxynitrite and their superoxide dismutase and catalase mimetic activity have been discussed recently (Walkey et al. 2015). The pectin-mediated nanoceria have been produced and evaluated for their antioxidant effect by using DPPH assay. For this assay, DPPH solution kept in the dark showed

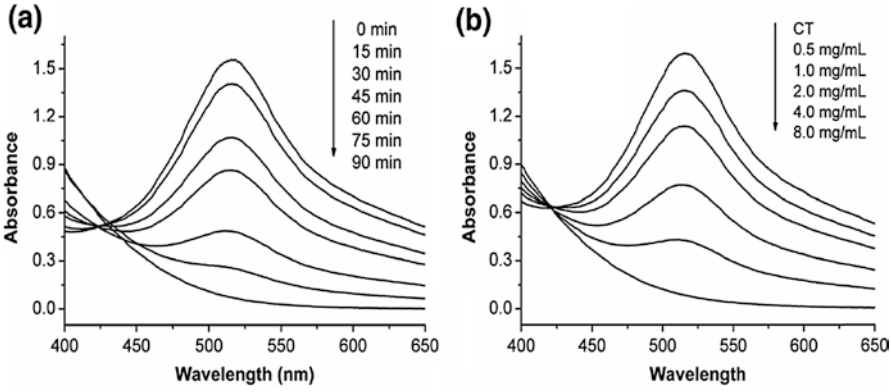

Fig. 10.13 Antioxidant activity of CeO NPs evaluated by the DPPH radical scavenging assay at (**a**) different intervals of time and (**b**) different concentrations (Patil and Paradeshi 2016)

unchanged intensity (517 nm) without any colour change, whereas in the presence of nanoceria, the absorption intensity was decreased with a colour change from deep violet to pale yellow (Fig. 10.13a). Figure 10.13b clearly indicates the decreased intensity with increase in the nanoceria concentration, and hence this decreased intensity is indicative of the free radical scavenging potential of nanoceria (Patil and Paradeshi 2016).

Nanoceria are also applicable for thermal decomposition and dye degradation. The nanoceria produced by using the *Azadirachta indica* leaf extract thermally decomposed ammonium perchlorate by dropping down the decomposition temperature of ammonium perchlorate by 130 °C and reducing the activation energy as well. This clearly indicated the excellent thermal catalytic behaviour of these NPs. On the other hand, their photocatalytic activity, having the degradation rate of 96% within 120 min, was revealed by photodegradation of Rhodamine B dye, indicating that they can be applied for dye degradation in wastewater treatment (Sharma et al. 2017).

10.6 Conclusions

Phytosynthesis of nanoparticles is an important and emerging area in nanoscience and technology. The several drawbacks of the conventional methods for NP synthesis have been overcome by the use of eco-friendly and novel green synthesis methods, which involve the use of plant extract, biopolymer and its derivatives, microbial derivatives and other natural products. Application of nanoceria is gaining ground in various fields despite many challenges. The different areas where nanoceria can be used include biosensing, plant science, coating, electronic applications, catalysis, biomedicine and nanomedicine, among others.

References

Annu AA, Ahmed S (2018) Green synthesis of metal, metal oxide nanoparticles, and their various applications. In: Martínez LMT, Kharissova OV, Kharisov BI (eds) Handbook of ecomaterials. Springer International Publishing, Cham, pp 1–45

Arumugam A, Karthikeyan C, Hameed ASH, Gopinath K, Gowri S (2015a) Synthesis of cerium oxide nanoparticles using *Gloriosa superba* L. leaf extract and their structural, optical and antibacterial properties. Mater Sci Eng C 49:408–415

Arumugam A, Karthikeyan C, Syedahamed A, Hameed ASH, Gopinath K, Gowri S, Karthika V (2015b) NU synthesis of cerium oxide nanoparticles using *Gloriosa superba*. Mater Sci Eng C Mater Biol Appl 49:408–415

Castano CE, O'Keefe MJ, Fahrenholtz WG (2015) Cerium-based oxide coatings. Curr Opin Solid State Mater Sci 19:69–76

Charbgoo F, Ahmad MB, Darroudi M (2017a) Cerium oxide nanoparticles: green synthesis and biological applications. Int J Nanomedicine 12:1401–1413

Charbgoo F, Ramezani M, Darroudi M (2017b) Bio-sensing applications of cerium oxide nanoparticles: advantages and disadvantages. Biosens Bioelectron 96:33–43
Dahle JT, Arai Y (2015) Environmental geochemistry of cerium: applications and toxicology of cerium oxide nanoparticles. Int J Environ Res Public Health 12:1253–1278
Darroudi M, Javad S, Kazemi R, Ali H (2014a) Food-directed synthesis of cerium oxide nanoparticles and their neurotoxicity effects. Ceram Int 40:7425–7430
Darroudi M, Sarani M, Oskuee RK, Zak AK, Hosseini HA, Gholami L (2014b) Green synthesis and evaluation of metabolic activity of starch mediated nanoceria. Ceram Int 40:2041–2045
Darroudi M, Sarani M, Oskuee RK, Zak AK, Amiri MS (2014c) Nanoceria: gum mediated synthesis and in vitro viability assay. Ceram Int 40:2863–2868
Dutta D, Mukherjee R, Patra M, Banik M, Dasgupta R, Mukherjee M, Basu T (2016) Green synthesized cerium oxide nanoparticle: a prospective drug against oxidative harm. Colloids Surf. B Biointerfaces 147:45–53
Enghag P (2004) The elements – origin, occurrence, discovery and names. In: Encyclopedia of the elements. Wiley-VCH Verlag GmbH & Co. KGaA, Weinheim, pp 55–78
Gao F, Lu Q, Komarneni S (2006) Fast synthesis of cerium oxide nanoparticles and nanorods. J Nanosci Nanotechnol 6:3812–3819
Gogoi A, Sarma KC (2017) Synthesis of the novel b -cyclodextrin supported CeO_2 nanoparticles for the catalytic degradation of methylene blue in aqueous suspension. Mater Chem Phys 194:327–336
Gopinath K, Karthika V, Sundaravadivelan C, Gowri S, Arumugam A (2015b) Mycogenesis of cerium oxide nanoparticles using *Aspergillus niger* culture filtrate and their applications for antibacterial and larvicidal activities. J Nanostruct Chem 5:295–303
Gusseme BDE, Laing GDU, Hennebel T, Renard P, Chidambaram D, Fitts JP, Bruneel E, Driessche IV, Verbeken K, Boon N, Verstraete W (2010) Virus removal by biogenic cerium. Environ Sci Technol 44:6350–6356
Hewer TLR, Soeira LS, Brito GES, Freire RS (2013) One-pot green synthesis of cerium oxide-carbon microspheres and their catalytic ozonation activity. J Mater Chem A 1:6169–6174
Hirano M, Fukuda Y, Iwata H, Hotta Y, Inagaki M (2000) Preparation and spherical agglomeration of crystalline cerium(IV) oxide nanoparticles by thermal hydrolysis. J Am Ceram Soc 83:1287–1289
Hirst SM, Karakoti AS, Tyler RD, Sriranganathan N, Seal S, Reilly CM (2009) Anti-inflammatory properties of cerium oxide nanoparticles. Small 5:2848–2856
Husen A (2017) Gold Nanoparticles from plant system: synthesis, characterization and their application. In: Ghorbanpour M, Manika K, Varma A (eds) Nanoscience and plant–soil systems, Springer, vol 48. Cham, Cham Switzerland, pp 455–479
Hussain I, Singh NB, Singh A, Singh H, Singh SC (2016) Green synthesis of nanoparticles and its potential application. Biotechnol Lett 38:545–560
Gopinath K, Karthika V, Sundaravadivelan C, Gowri S, Arumugam A (2015a) Mycogenesis of cerium oxide nanoparticles using *Aspergillus niger* culture filtrate and their applications for antibacterial and larvicidal activities. J Nanostruct Chem 5:295–303
Kannan SK, Sundrarajan M (2014) A green approach for the synthesis of a cerium oxide nanoparticle: characterization and antibacterial activity. Int J Nanosci 13:1450018
Kargar H, Ghasemi F, Darroudi M (2014) Bioorganic polymer-based synthesis of cerium oxide nanoparticles and their cell viability assays. Ceram Int 41:1589–1594
Kargar H, Ghasemi F, Darroudi M (2015) Bioorganic polymer-based synthesis of cerium oxide nanoparticles and their cell viability assays. Ceram Int 41:1589–1594
Khan SA, Ahmad A (2013) Fungus mediated synthesis of biomedically important cerium oxide nanoparticles. Mater Res Bull 48:4134–4138
Kilbourn BT (2000) Cerium and cerium compounds. Kirk-Othmer encyclopedia of chemical technology. Wiley, New York, In
Kumar E, Selvarajan P, Muthuraj D (2013) Synthesis and characterization of CeO_2 nanocrystals by solvothermal route. Mater Res 16:269–276

Li B, Chen Y, Liang W. Mu L, Bridges WC, Jacobson AR, Darnault CJG (2017) Influence of cerium oxide nanoparticles on the soil enzyme activities in a soil-grass microcosm system. Geoderma 299:54–62

Maensiri S, Masingboon C, Laokul P, Jareonboon W, Promarak V, Anderson PL, Seraphin S (2007) Egg white synthesis and photoluminescence of platelike clusters of CeO_2 nanoparticles. Cryst Growth Des 7:950–955

Malleshappa J, Nagabhushana H, Sharma SC, Vidya YS, Anantharaju KS, Prashantha SC, Daruka Prasad B, Raja Naika H, Lingaraju K, Surendra BS (2015) *Leucas aspera* mediated multifunctional CeO_2 nanoparticles: structural, photoluminescent, photocatalytic and antibacterial properties. Spectrochim Acta A Mol Biomol Spectrosc 149:452–462

Masui T, Hirai H, Imanaka N, Adachi G, Sakata T, Mori H (2002) Synthesis of cerium oxide nanoparticles by hydrothermal crystallization with citric acid. J Mater Sci Lett 21:489–491

Mittal S, Pandey AK (2014) Cerium oxide nanoparticles induced toxicity in human lung cells: role of ROS mediated DNA damage and apoptosis. Biomed Res Int 2014:1–14

Munusamy S, Bhakyaraj K, Vijayalakshmi L, Stephen A, Narayanan V (2014) Synthesis and characterization of cerium oxide nanoparticles using *Curvularia lunata* and their antibacterial properties. Int J Innov Res Sci Eng 2:318–323

Nguyen D, Visvanathan C, Jacob P, Jegatheesan V (2015) Effects of nano cerium (IV) oxide and zinc oxide particles on biogas production. Int Biodeter Biodegr 102:165–171

Oró D, Yudina T, Fernández-Varo G, Casals E, Reichenbach V, Casals G, González de la Presa B, Sandalinas S, Carvajal S, Puntes V, Jiménez W (2016) Cerium oxide nanoparticles reduce steatosis, portal hypertension and display anti-inflammatory properties in rats with liver fibrosis. J Hepatol 64:691–698

Patil SN, Paradeshi JS (2016) Bio-therapeutic potential and cytotoxicity assessment of pectin-mediated synthesized nanostructured cerium oxide. Appl Biochem Biotechnol 638–654

Perez JM, Asati A, Nath S, Kaittanis C (2008) Synthesis of biocompatible dextran-coated Nanoceria with pH-dependent antioxidant properties. Small 4:552–556

Pinjari DV, Pandit AB (2011) Room temperature synthesis of crystalline CeO_2 nanopowder: advantage of sonochemical method over conventional method. Ultrason Sonochem 18:1118–1123

Primo A, Marino T, Corma A, Molinari R, García H (2011) Efficient visible-light photocatalytic water splitting by minute amounts of gold supported on nanoparticulate CeO_2 obtained by a biopolymer templating method. J Am Chem Soc 133:6930–6933

Priya GS, Kanneganti A, Kumar KA, Venkateswara Rao K, Bykkam S (2014) Biosynthesis of cerium oxide nanoparticles using Aloe barbadensis miller gel. Int J Sci Res Publ 4:199–224

Qian J, Chen F, Zhao X, Chen Z (2011) China rose petal as biotemplate to produce two-dimensional ceria nanosheets. J Nanopart Res 13:7149–7158

Reddy Yadav LS, Manjunath K, Archana B, Madhu C, Raja Naika H, Nagabhushana H, Kavitha C, Nagaraju G (2016) Fruit juice extract mediated synthesis of CeO2 nanoparticles for antibacterial and photocatalytic activities. Eur Phys J Plus 131:154

Rocca A, Moscato S, Ronca F, Nitti S, Mattoli V, Giorgi M, Ciofani G (2015) Pilot in vivo investigation of cerium oxide nanoparticles as a novel anti-obesity pharmaceutical formulation. Nanomedicine: Nanotechnol Biol Med 11:1725–1734

Sankar V, SalinRaj P, Athira R, Soumya RS, Raghu KG (2015) Cerium nanoparticles synthesized using aqueous extract of *Centella asiatica*: characterization, determination of free radical scavenging activity and evaluation of efficacy against cardiomyoblast hypertrophy. RSC Adv 5:21074–21083

Sathiyanarayanan G, Dineshkumar K, Yang YH (2017) Microbial exopolysaccharide-mediated synthesis and stabilization of metal nanoparticles. Crit Rev Microbiol 43:731–752

Sharma JK, Srivastava P, Ameen S, Akhtar MS, Sengupta SK, Singh G (2017) Phytoconstituents assisted green synthesis of cerium oxide nanoparticles for thermal decomposition and dye remediation. Mater Res Bull 91:98–107

Siddiqi KS, Husen A (2017) Recent advances in plant-mediated engineered gold nanoparticles and their application in biological system. J Trace Elem Med Biol 40:10–23

Siddiqi KS, Husen A, Rao RAK (2018) A review on biosynthesis of silver nanoparticles and their biocidal properties. J Nanobiotechnology 16:14

Sifontes AB, Gonzalez G, Ochoa JL et al (2011) Chitosan as template for the synthesis of ceria nanoparticles. Mater Res Bull 46:1794–1799

Sun C, Li H, Chen L (2012) Nanostructured ceria-based materials: synthesis, properties and applications. Energy Environ Sci 5:8475–8505

Tamizhdurai P, Sakthinathan S, Chen SM, Shanthi K, Sivasanker S, Sangeeth P (2017) Environmentally friendly synthesis of CeO_2 nanoparticles for the catalytic oxidation of benzyl alcohol to benzaldehyde and selective detection of nitrite. Sci Rep 7:46372

Trovarelli A, de Leitenburg C, Boaro M, Dolcetti G (1999) The utilization of ceria in industrial catalysis. Catal Today 50:353–367

Vinothkumar G, Amalraj R, Babu KS (2017) Fuel-oxidizer ratio tuned luminescence properties of combustion synthesized Europium doped cerium oxide nanoparticles and its effect on antioxidant properties. Ceram Int 43:5457–5466

Walkey C, Das S, Seal S, Erlichman J, Heckman K, Ghibelli L, Traversa E, McGinnis JF, Self WT (2015) Catalytic properties and biomedical applications of cerium oxide nanoparticles. Environ Sci Nano 2:33–53

Weeks ME (1932) The discovery of the elements. XVI. The rare earth elements. J Chem Educ 9:1751

Yin L, Wang Y, Pang G et al (2002) Sonochemical synthesis of cerium oxide nanoparticles—effect of additives and quantum size effect. J Colloid Interface Sci 246:78–84

Zhang F, Chan S-W, Spanier JE, Apak E, Jin Q, Robinson RD, Herman IP (2002) Cerium oxide nanoparticles: size-selective formation and structure analysis. Appl Phys Lett 80:127–129